

# Modeling HA-protein mediated interaction between an influenza virus and a healthy cell: pre-fusion membrane deformation

Naveen Vaidya<sup>1</sup>, Huaxiong Huang<sup>1</sup>, and Shu Takagi<sup>2</sup>

<sup>1</sup>Department of Mathematics and Statistics, York University, Toronto, Canada M3J 1P3

<sup>2</sup>Department of Mechanical Engineering, The University of Tokyo, Tokyo, Japan

August 25, 2006

## Abstract

We present a mathematical model for pre-fusion interaction between an influenza virus and a healthy cell. The model describes the role of the force exerted by Hemagglutinin (HA) protein clusters in bringing the viral membrane in close contact with the host cell membrane, as a first step of the fusion process between the two membranes. We model the viral membrane as a lipid bilayer whose shape energy is given by the Helfrich functional. Using the calculus of variation, we compute the deformation of the viral membrane under the influence of the protein force. Our numerical results support the hypothesis of dimple formation in the fusion-site proposed in the literature. We discuss the effects of spontaneous curvature, protein-cluster radius, fusion-site radius and protein-cluster force on the dimple size/shape and the energy stored. We also examine the effects of membrane incompressibility and the presence of the host cell on the dimple shape. Our results on the effects of the membrane incompressibility property and spontaneous curvature support the experimental results.

**Key words:** Viral membrane fusion; Lipid bilayer; Equilibrium membrane shape; Euler-Lagrange equation.

# 1 Introduction

The first step for the invasion of an influenza virus into a healthy cell is the fusion of the membranes mediated by Hemagglutinin (HA) protein. Despite variations in localization, timing and frequency in the fusion process, due to varieties in fusion-protein, two lipid bilayers of the virus and the host cell eventually merge in the end [2, 15, 19, 34, 39]. In order for fusion to occur, the two lipid bilayers have to be brought into a close contact. On the other hand, when an influenza virus first attaches to the viral receptor containing sialic acid of the target membrane with the help of HA-spike tip, the viral membrane and the target membrane are separated by 13.5 nm (the height of the viral spike protein) [36, 39], which is too far for fusion to occur. Understanding the pre-fusion mechanism in which HA-protein brings two membranes close to each other is important for various purposes such as disease control and drug design.

In modeling the fusion mechanism, most efforts have been put into the study of an intermediate structure called fusion stalk (a local lipidic connection between the proximal i.e. contacting monolayers of the fusing membranes) [16, 17, 18, 21, 24, 39]. The main focus is on building models so that the predicted energy in the stalk reaches a physically reasonable level (i.e. to make the energy required sufficiently low) while assuming that there exists a source of energy required to form a stalk. In fact, the main source of the energy for the stalk formation is the energy accumulated during the pre-fusion process. Therefore, it is important to study of the dependence of energy on various parameters such as protein-force, protein-cluster size, fusion-site size etc. during pre-fusion since that will shed lights on the possibility of stalk formation as an intermediate stage of the fusion process and consequently, the possibility of a successful fusion process. The result will be useful for the purpose of drug design as the general idea behind modern antiviral drug design is to identify viral proteins, or parts of proteins, that can be disabled. Despite being an important component of the fusion process, the pre-fusion process has not received much attention until recent years [15, 19].

In [15], it was hypothesized that the activated HA-protein can produce viral membrane dimples surrounded by a ring-like cluster of HA. Assuming that the top of the dimple is a segment of perfect sphere connected to a funnel of a catenoid form (an axisymmetric surface with zero total curvature), it was argued

that the energy involved in the process is sufficient to cause instability of the lipid bilayers. Similarly, perfectly spherical shape of the top of the dimple (nipple in their word) has been assumed in the calculation of the energy [19]. Moreover, the dimpling has been accepted in [23] as the means for membranes to make the intimate contact, which is required for fusion.

In this study, we propose a model for pre-fusion membrane deformation, in the form of an energy functional. Our model incorporates the energy contribution due to the bending rigidity of the membrane and the energy due to HA-protein. Our main objective is to verify the hypothesis of dimple formation [15, 19, 23], without assuming a specific shape of the viral membrane. Our numerical results confirm the dimple formation as well as the extra energy accumulated inside the dimple area.

The lipid bilayer is nearly incompressible and experimental work [23] has found that the tension created in the membranes inhibits fusion. This shows that membrane compressibility, which was neglected in previous studies [15, 19], may play a crucial role in the fusion/pre-fusion process. Therefore, we also examine the effect of membrane compressibility during pre-fusion process by incorporating membrane compressibility into our model. Our result is consistent with the experimental result in [23]. When the dimple forms, the presence of the host cell membrane may also have an effect on the viral membrane deformation. We further extend our original model to investigate the impact of the host membrane on the growing dimple as well as the effects of spontaneous curvature, fusion-site radius, protein-cluster radius and protein-force on the dimple shape/size and the energy stored inside the dimple. Effect of the spontaneous curvature predicted by our model is in a good agreement with the experimental observations [23].

The rest of the paper proceeds as follows. We present the model in Section 2. Axisymmetric shape equations of viral membrane (with and without incompressibility) and the extension to include cell-membrane interaction are given in Section 3. A brief description of the solution method is given in Section 4, which is followed by the discussion of results in Section 5. We conclude the paper in Section 6.

## 2 Model

Even though the influenza viral membrane consists of two types of protein, hemagglutinin (HA) and neuraminidase, it has been suggested that HA is the one which facilitates the fusion of the lipid bilayers [30]. Therefore, we consider only HA protein in our model. HA is a glycoprotein which consists of a trimer with individual monomer having HA1 and HA2 subunits [2, 9, 15, 20, 22, 32, 33, 34]. It is believed that HA1 is responsible for virus attachment to the cell surface via sialic acid binding site and HA2 activates the fusion process. During low-pH-activation (i.e. when the protein is exposed to pH 5) the hydrophobic fusion peptide previously hidden within the trimeric stem is projected towards viral and/or target membranes [2, 8, 15, 29]. The subsequent refolding of the protein exerts a force on the fusion peptide inserted into the membrane. Even though a similar process takes place in the target membrane due to protein force (via inserted fusion peptide), for simplicity we focus only on the viral membrane in this study.

We assume that the viral membrane can resist bending and the shape of the membrane is determined by minimizing a Helfrich-type energy functional. It was proposed in [15] that the protein clusters form a ring. Within each cluster, the protein exerts a bending force on the membrane, causing the membrane to deform into a saddle-like shape with two principle curvatures  $c_1 = -c_2 = c_p$ . Thus the total contribution of the protein cluster to the membrane energy is given by integrating  $\tau_p c_p$  over the cluster area, where  $\tau_p$  is a bending moment applied by the protein to the unit length of the circumference of the membrane fragment. In this paper, we relaxed the assumption in [15], without imposing the saddle shape *a priori*. Instead, we assume that the bending forces act on both principle directions and we consider the dependence of the energy contribution due to protein force only up to the first order term of the curvature (i.e. linear dependence). In principle, the forces acting on two principle directions need not be related. However, to simplify the discussion, we assume that they are of the same magnitude and the energy functional takes the form

$$E = \frac{1}{2}k_b \int (c_1 + c_2 - c_0)^2 dA + k_G \int c_1 c_2 dA + \int f_p (c_1 - c_2) dA. \quad (2.1)$$

Here the first two terms are Helfrich [11] energy due to the bending rigidity and Gaussian bending rigidity of the membrane respectively. The last term is energy contribution due to the work by the protein force.

$dA$ ,  $k_b$  and  $k_G$  are surface area element, bending rigidity and Gaussian bending rigidity, respectively;  $c_1$  and  $c_2$  denote two principal curvatures and  $c_0$  denotes the spontaneous curvature which takes the possible asymmetry of the bilayer into account;  $f_p$  is the force exerted by HA-protein on the membrane. Motivation for introducing the energy due to protein-cluster as the third term in (2.1) is that due to the force exerted by the protein-cluster, we expect the tendency of curvatures  $c_1$  and  $c_2$  of the membrane segment in the protein-cluster region to be negative and positive respectively so that the total work performed by the protein-cluster  $\int f_p(c_1 - c_2)dA$  is negative. We note that as a special case of  $k_G = 0$ ,  $c_0 = 0$ ,  $c_1 = -c_2 = c_p$  and  $f_p = -\tau_p/2$ , our model produces the saddle-like shape of the membrane fragment hypothesized in [15].

As shown by the experimental observations [23] that the tension developed in the membranes inhibits fusion. This suggests that the compressibility of the lipid bilayer membrane may have considerable impact in pre-fusion process. Exchange of molecules between the membrane and the environment takes place through desorption and adsorption. However, these processes occur much slower than the prefusion events investigated here. Hence the number of molecules in the membrane remains globally almost constant [14] and the biological membranes consisting of lipid bilayers can be treated as two-dimensional nearly-incompressible media [26, 27]. This results in a local surface area constraint which applies to the entire cell as well as membrane fragment even though the individual lipid molecules can move almost freely. In reality there are also factors such as transmembrane domains of the fusion protein restricting lipid delivery to the membrane [16]. However, this effect will not be considered here. Membrane incompressibility is incorporated by adding a term into the model as follows

$$E = \frac{1}{2}k_b \int (c_1 + c_2 - c_0)^2 dA + k_G \int c_1 c_2 dA + \int f_p(c_1 - c_2)dA + \gamma \int dA, \quad (2.2)$$

where  $\gamma$  is an in-plane tension developing to ensure membrane incompressibility, i.e., preserving the surface area of the membrane. In this study, since the area of the membrane segment is not fixed in our setup, the value of  $\gamma$  will be given in the computation. The prescribed value of  $\gamma$  can be viewed as a measure of the compressibility of the membrane. In the following sections, we will discuss how to compute the pre-fusion deformation of the viral membrane, based on the energy functional given by equations (2.1) and (2.2).

### 3 Axisymmetric shape equation of viral membrane

#### 3.1 Shape equation without constraints

The deformation of the membrane shape without constraints can be computed by minimizing the energy (2.1) directly. In this paper, we use an indirect method by deriving Euler-Lagrange equation (so-called shape equation in the physics literature) first. Since our objective is to model and analyze the membrane behavior during the pre-fusion state without the merging of the viral and the host cell membranes, the viral membrane does not experience topological change. This allows us to drop the Gaussian curvature term in (2.1). We now consider the axisymmetric viral membrane with the axis of symmetry along the  $z$ -axis and  $s$ ,  $\rho$ ,  $\psi$  are the arc-length of the contour, the distance to the symmetric axis and the angle made by the tangent to the contour with the plane perpendicular to the axis of symmetry respectively (See Fig. 1). Here, the coordinates  $z(s)$  and  $\rho(s)$  have to satisfy the geometrical relations:

$$\frac{d\rho}{ds} = \cos \psi \tag{3.1}$$

$$\frac{dz}{ds} = -\sin \psi. \tag{3.2}$$

There are a number of ways the axisymmetric shape equation can be derived. Obviously, one can try to derive the general shape equation in 3D by modifying the approach in [38] and apply the condition of axisymmetry. A more appealing alternative is to work with the axisymmetric form of the energy functional before applying calculus of variation. However, there have been some concerns and confusions related to this approach [4, 12, 25, 27] and it has been argued in [12] that the variation has to be performed in the normal direction to obtain the correct shape equation. To clarify some of the confusion, we have addressed the issue regarding the derivation of the correct Euler-Lagrange equation in this paper. We have shown that the variation in the direction perpendicular to the axis of symmetry can also produce the correct shape equation if the induced variation in other variables are obtained by using the geometric relations  $d\rho/ds = \cos \psi$  and  $dz/ds = -\sin \psi$ . Therefore, the variation does not have to be in the normal direction. We have further

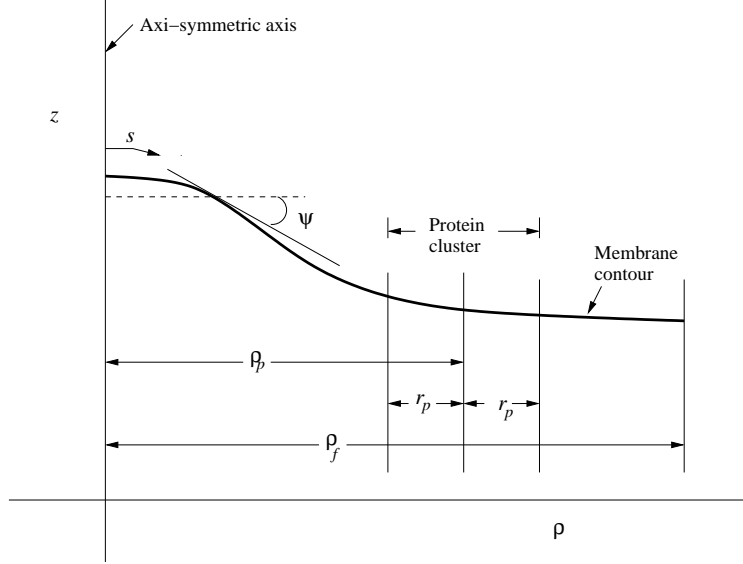


Figure 1: Schematic diagram of the axisymmetric viral membrane.

proved that to obtain the correct shape equation of the axisymmetric membrane by finding Euler-Lagrange equations, we need to maintain the geometric constraint  $\cos \psi (dz/d\rho) + \sin \psi = 0$  while performing the variation. We refer the readers to the Appendix for the proofs of the above mentioned results.

Therefore, we can obtain the correct axisymmetric shape equations of the viral membrane by using the geometric constraint and obtaining Euler-Lagrange equations. Using axisymmetric curvatures

$$c_1 = \cos \psi \frac{d\psi}{d\rho}, \quad c_2 = \frac{\sin \psi}{\rho}, \quad \text{and} \quad \cos \psi \frac{dz}{d\rho} + \sin \psi = 0$$

via a Lagrangian multiplier  $\eta$ , the energy functional (2.1) can be written as

$$F = \pi \int_0^{\rho_f} \mathcal{L} d\rho, \quad (3.3)$$

where

$$\begin{aligned} \mathcal{L} = & k_b \rho \cos \psi \left( \frac{d\psi}{d\rho} \right)^2 + 2k_b \sin \psi \frac{d\psi}{d\rho} + \frac{k_b \sin^2 \psi}{\rho \cos \psi} + 2f_p \rho \frac{d\psi}{d\rho} - \frac{2f_p \sin \psi}{\cos \psi} \\ & + \frac{k_b \rho c_0^2}{\cos \psi} - 2c_0 k_b \rho \frac{d\psi}{d\rho} - \frac{2k_b c_0 \sin \psi}{\cos \psi} + \eta \left( \cos \psi \frac{dz}{d\rho} + \sin \psi \right) \end{aligned} \quad (3.4)$$

and  $\rho_f$  is the maximum distance of the membrane considered from the axis of symmetry.

Using calculus of variation, from the energy functional (3.3), we can derive the following Euler-Lagrange equations

$$\begin{aligned} \cos^2 \psi \frac{d^2 \psi}{d\rho^2} = & \frac{\sin 2\psi}{4} \left( \frac{d\psi}{d\rho} \right)^2 + \frac{\sin 2\psi}{4\rho^2} + \frac{\sin \psi}{2\rho^2 \cos \psi} - \frac{\cos^2 \psi}{\rho} \frac{d\psi}{d\rho} - \frac{f_p}{k_b \rho} \left( \cos \psi + \frac{1}{\cos \psi} \right) \\ & - \frac{\cos \psi}{k_b} \frac{df_p}{d\rho} - \frac{\eta_0}{2k_b \rho \cos \psi} + \frac{c_0^2 \sin \psi}{2 \cos \psi} - \frac{c_0 \sin^2 \psi}{\rho \cos \psi}, \end{aligned} \quad (3.5)$$

$$\cos \psi \frac{dz}{d\rho} = -\sin \psi, \quad (3.6)$$

$$\eta \cos \psi = \eta_0 \quad (3.7)$$

where  $\eta_0$  is an integrating constant.

For the fusion to occur, during conformational change at low pH, interaction between adjacent HA trimers with high local density results in multiple trimer assemble around the fusion site [22]. These assembled HA trimers can be assumed to form ring-like clusters surrounding the fusion site [1, 3, 6, 15, 39] and these proteins perform concerted activation to synchronously release the conformational energy [22]. Moreover, fusion peptide interaction among neighboring HAs has been hypothesized to be responsible for a measurable decrease in lateral mobility of HA after activation [10, 22]. Based on these observation, we assume that HA trimmers are axisymmetrically distributed on a ring formed about the axis of symmetry of the membrane. Then the force  $f_p$  exerted by the protein is given by

$$f_p(\rho) = F_p H(\rho),$$

where Heavside function  $H(\rho)$  is

$$H(\rho) = \begin{cases} 1, & \text{if } |\rho - \rho_p| \leq r_p; \\ 0, & \text{otherwise.} \end{cases}$$

Here,  $F_p$ ,  $\rho_p$  and  $r_p$  are magnitude of the force exerted by protein, average of the internal and external radii of the protein ring and half of the thickness of the protein ring respectively. The derivative of the heaviside

function is a delta function, so the derivative of  $f_p(\rho)$  is given by

$$\frac{df_p}{d\rho} = \begin{cases} 0, & 0 \leq \rho < (\rho_p - r_p); \\ \infty, & \rho = (\rho_p - r_p); \\ 0, & (\rho_p - r_p) < \rho < (\rho_p + r_p); \\ -\infty, & \rho = (\rho_p + r_p); \\ 0, & (\rho_p + r_p) < \rho \leq \rho_f. \end{cases}$$

### 3.2 Boundary conditions

Let  $\rho_f$  be the distance from the axis of symmetry where the membrane remains undisturbed i.e the membrane remains horizontal (flat). To avoid a corner at the axis of symmetry, we use symmetry condition  $dz/d\rho = 0$  at  $\rho = 0$ . And  $dz/d\rho = -\tan \psi$  implies  $\psi = 0$  at  $\rho = 0$ . Membrane being horizontal at  $\rho = \rho_f$  gives the condition  $\psi(\rho_f) = 0$ . Therefore, to solve shape equations (3.5) and (3.6) we use the following boundary conditions.

$$\rho = 0 : \quad \psi = 0 \tag{3.8}$$

$$\rho = \rho_f : \quad \psi = 0, \frac{d\psi}{d\rho} = 0, z = z_f,$$

where  $z_f$  is arbitrary. Since we need an extra boundary condition due to presence of unknown  $\eta_0$ , we have added a no-flux type of boundary condition  $d\psi/d\rho = 0$  for the point where membrane remains undisturbed (horizontal).

### 3.3 Shape equation for incompressible membranes

Imposing the axisymmetric relations in the energy functional (2.2), we get the following action form

$$F_{in} = \pi \int_0^{\rho_f} [\mathcal{L} + 2\gamma\rho \sec \psi] d\rho. \tag{3.9}$$

This functional leads the following Euler-Lagrange equations

$$\begin{aligned} \cos^2 \psi \frac{d^2 \psi}{d\rho^2} &= \frac{\sin 2\psi}{4} \left( \frac{d\psi}{d\rho} \right)^2 + \frac{\sin 2\psi}{4\rho^2} + \frac{\sin \psi}{2\rho^2 \cos \psi} - \frac{\cos^2 \psi}{\rho} \frac{d\psi}{d\rho} - \frac{f_p}{k_b \rho} \left( \cos \psi + \frac{1}{\cos \psi} \right) \\ &\quad - \frac{\cos \psi}{k_b} \frac{df_p}{d\rho} - \frac{\eta_0}{2k_b \rho \cos \psi} + \frac{c_0^2 \sin \psi}{2 \cos \psi} - \frac{c_0 \sin^2 \psi}{\rho \cos \psi} + \frac{\gamma \sin \psi}{k_b \cos \psi}, \end{aligned} \tag{3.10}$$

$$\cos \psi \frac{dz}{d\rho} = -\sin \psi, \quad (3.11)$$

$$\eta \cos \psi = \eta_0 \quad (3.12)$$

### 3.4 Presence of cell membrane

So far we have ignored possible interaction between the viral and the host cell membranes. As the two membranes are brought into close distance, we need to consider the deformation of both. To simplify the discussion, we assume that the host membrane is rigid. As a result, we have a contact problem, which can be treated under our general framework by imposing an additional constraint. As a simple model, we incorporate the presence of target membrane as an opposing surface for the viral membrane via an inequality

$$z \leq z_h. \quad (3.13)$$

Here,  $z_h$  is the vertical height of the horizontal host cell membrane from the  $\rho$ -axis, where the virus meets the host cell.

Following [28], we implement the inequality constraint by changing it into the equality constraint as  $z_h - z = \xi^2$ . Again, we apply this equality constraint via a Lagrangian multiplier so that the energy functional becomes

$$F_h = \int_0^{\rho_f} [\pi \mathcal{L} + \zeta(z - z_h + \xi^2)] d\rho. \quad (3.14)$$

The corresponding Euler-Lagrange equations are

$$\begin{aligned} \cos^2 \psi \frac{d^2 \psi}{d\rho^2} &= \frac{\sin 2\psi}{4} \left( \frac{d\psi}{d\rho} \right)^2 + \frac{\sin 2\psi}{4\rho^2} + \frac{\sin \psi}{2\rho^2 \cos \psi} - \frac{\cos^2 \psi}{\rho} \frac{d\psi}{d\rho} - \frac{f_p}{k_b \rho} \left( \cos \psi + \frac{1}{\cos \psi} \right) \\ &\quad - \frac{\cos \psi}{k_b} \frac{df_p}{d\rho} - \frac{\eta}{2k_b \rho} + \frac{c_0^2 \sin \psi}{2 \cos \psi} - \frac{c_0 \sin^2 \psi}{\rho \cos \psi}, \end{aligned} \quad (3.15)$$

$$\cos \psi \frac{d\eta}{d\rho} = \zeta + \eta \sin \psi \frac{d\psi}{d\rho}, \quad (3.16)$$

$$\cos \psi \frac{dz}{d\rho} = -\sin \psi, \quad (3.17)$$

$$z - z_h = -\xi^2, \quad (3.18)$$

$$\zeta \xi = 0. \quad (3.19)$$

Simple manipulations show that equations (3.17) and (3.18) can be replaced by the following equation

$$2\xi \cos \psi \frac{d\xi}{d\rho} = \sin \psi. \quad (3.20)$$

Equations (3.15), (3.16), (3.19) and (3.20) can be solved using boundary conditions  $\psi(0) = 0, \psi(\rho_f) = 0, \eta(0) = 0, \xi(\rho_f) = \sqrt{z_h - z_f}$ . Notice that  $\eta \cos \psi$  is no longer a constant in this case.

## 4 Solution methodology

In this section we briefly explain how to solve Euler-Lagrange equations derived earlier. We will use system (3.5) and (3.6) as an example as the method for (3.10) and (3.11) as well as (3.15), (3.16), (3.19) and (3.20) are similar. To solve the system of ordinary differential equations (3.5) and (3.6) with boundary conditions (3.8), we use the finite difference method. At the boundaries in which Neumann's boundary conditions are given, we determine numerically the boundary values by using Taylor expansion with the given boundary conditions. We use the following numerical scheme to solve the system (3.5) and (3.6).

Let  $\Delta\rho = \rho_f/(N+1)$  be the spatial step-size so that  $\rho_i = i\Delta\rho, i = 0, 1, 2, \dots, (N+1)$  is the partition of  $[0, \rho_f]$ . We assume that  $\psi_i$  and  $z_i$  are approximations to  $\psi$  and  $z$  respectively at the grid point  $\rho_i, i = 1, 2, \dots, N$ . In this uniform mesh grid we use the following discretization

$$\begin{aligned} \left. \frac{d^2\psi}{d\rho^2} \right|_{\rho_i} &= \frac{\psi_{i+1} - 2\psi_i + \psi_{i-1}}{(\Delta\rho)^2}, \\ \left. \frac{d\psi}{d\rho} \right|_{\rho_i} &= \frac{\psi_{i+1} - \psi_{i-1}}{2\Delta\rho}, \\ \left. \frac{dz}{d\rho} \right|_{\rho_i} &= \frac{z_{i+1} - z_i}{\Delta\rho}. \end{aligned}$$

And the system (3.5)-(3.6) can be discretized as

$$\begin{aligned} &\cos^2 \psi \left[ \frac{\psi_{i+1} - 2\psi_i + \psi_{i-1}}{(\Delta\rho)^2} \right] - \frac{\sin 2\psi_i}{4} \left[ \frac{\psi_{i+1} - \psi_{i-1}}{\Delta\rho} \right]^2 - \frac{\sin 2\psi_i}{4\rho_i^2} - \frac{\sin \psi_i}{2\rho_i^2 \cos \psi_i} \\ &- \frac{\cos^2 \psi_i}{\rho_i} \left[ \frac{\psi_{i+1} - \psi_{i-1}}{2\Delta\rho} \right] + \frac{f_p(\rho_i)}{k_b \rho_i} \left( \cos \psi_i + \frac{1}{\cos \psi_i} \right) + \frac{\cos \psi_i}{k_b} \left. \frac{df_p}{d\rho} \right|_{\rho_i} + \frac{\eta_0}{2k_b \rho_i \cos \psi_i} \\ &- \frac{c_0^2 \sin \psi_i}{2 \cos \psi_i} + \frac{c_0 \sin^2 \psi_i}{\rho_i \cos \psi_i} = 0, \end{aligned}$$

$$\begin{aligned} \cos \psi_i \frac{z_{i+1} - z_i}{\Delta \rho} + \sin \psi_i &= 0, \\ i &= 1, 2, \dots, N. \end{aligned} \quad (4.1)$$

Using the boundary conditions (3.8), this scheme produces a nonlinear system of  $2N - 1$  equations with  $2N - 1$  unknowns  $\psi_1, \psi_2, \dots, \psi_{N-1}, z_1, z_2, \dots, z_{N-1}, \eta_0$ . This non-linear system of algebraic equations is solved by the Gauss-Newton method with line search.

## 5 Result and discussion

One of the objectives of this paper is to confirm the hypothesis proposed in [15] that the distance between the viral and cell membranes could be reduced significantly to facilitate fusion by forming “dimples”, due to the bending force exerted by the protein clusters. We start by discussing the results for the case with no constraints.

### 5.1 Deformation without constraints

In reality, the value of  $\rho_f$  where the membrane becomes flat depends upon the density of the activated HA trimers. As mentioned in [15], the contact area of radius  $\sim 25$  nm can have  $\sim 10$  dimples if all HA molecules in this area are activated. This helps to estimate the range of  $\rho_f$  to be from 8 nm to 25 nm. Therefore, for the purpose of our computation, we consider  $\rho_f = 20$  nm.

For the comparison purpose, we have carried out the simulation with the same values  $k_b = 20$  kT,  $f_p = 2.4 \times 10^{-11}$  N,  $c_0 = 0$ ,  $\rho_p = 8$  nm and  $r_p = 4$  nm, i.e., the radius of the fusion-site  $(\rho_p - r_p) = 4$  nm as in [15]. By assuming that the dimple top is spherical, they predict that the angle  $\psi$  at the end of the dimple top is approximately 0.6 and that the top is the segment of the sphere of radius 7.0841 nm. We plot this segment (dot-dashed line) along with the dimple top predicted using our model in Fig. 2(a). It can be seen that the spherical shape gives a reasonable approximation of the dimple top. However, the overall shape of the membrane deformation predicted by our model, differs from the sphere. This can be seen more clearly in Fig. 2(b), where the two principle curvatures are plotted. Near the axis of symmetry

$c_1$  and  $c_2$  are close to each other showing the approximate spherical shape. However, the curvatures are not constant and as it gets away from the axis of symmetry, the difference between them gets larger and larger showing the deviation from the spherical shape. Moreover, the total curvature does not vanish in the protein-cluster region, specially closer to the dimple-top. This result is contrary to catenoid shape of the membrane in the protein-cluster region hypothesized in [15]. The distribution of the energy contribution by the bending rigidity term and the protein force term is plotted in Fig. 2(c). Only term contributing in the dimple-top is obviously the bending rigidity term due to absence of protein inside the fusion-site. However, in the protein-cluster region, the dominating contribution to the energy comes from the protein force.

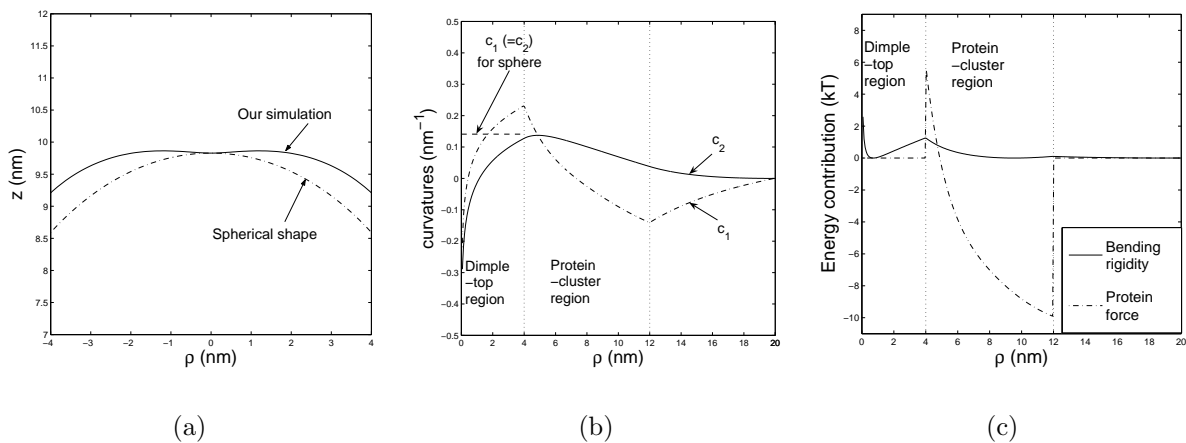


Figure 2: (a) Comparison of the shape of the dimple top of the viral membrane with the spherical shape (b) Principal curvatures distribution of the viral membrane (c) Energy contribution due to bending rigidity and due to protein force.

In order to facilitate fusion, a significant amount of energy must be available for the merge of the monolayers. Our computation shows that the energy stored in the dimple-top is 37.43 kT. Here, the height of the dimple-top from the horizontal membrane plane is 9.8 nm. The energy predicted by our model is reasonable compared to the energy required ( $\approx 37\text{kT}$ ) for the merging of monolayers [19, 21]. Since the sufficient amount of energy can be stored in the dimple-top to carry out the fusion process, the dimple formation mechanism due to protein cluster to bring the membranes closer to each other during pre-fusion is acceptable.

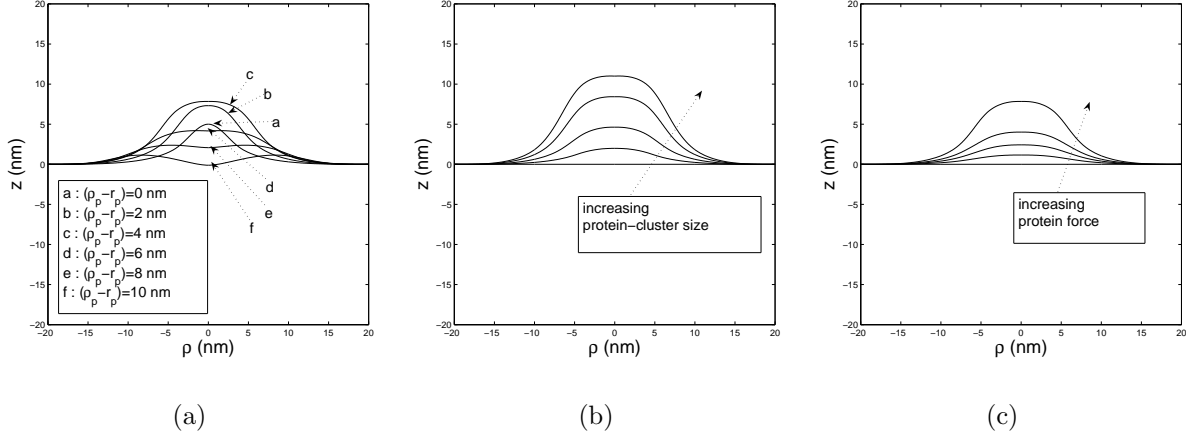


Figure 3: Contour shape of the viral membrane for (a) the different fusion-site radius (b) the different protein-cluster thickness (c) the different protein force.

In Fig. 3(a) we plot the membrane shape as we vary the radius of the fusion-site ( $\rho_p - r_p$ ). The graph shows that there is a maximum dimple height as a function of the fusion-site radius. It should be noted that for some values of ( $\rho_p - r_p$ ), the membrane even forms a small reverse dimple at the axis of symmetry. This shows that the assumption of spherical top of the dimple is not acceptable all the times. For a successful fusion to occur, there may exist an optimal value of ( $\rho_p - r_p$ ) for the HA-molecules to form clusters. This can be illustrated further by examining the energy stored in the membrane. For  $f_p = 2 \times 10^{-11}$  N,  $c_0 = 0$  and  $r_p = 2$  nm, the energy stored in the dimple and the total bending energy as a function of the fusion-site radius ( $\rho_p - r_p$ ) are plotted in Figs. 4(b) and 5(b), respectively. Here, the total bending energy stored in the membrane is computed by integrating the bending energy on the entire membrane (i.e up to  $\rho = \rho_p + r_p$ ) and the energy stored in the dimple-top is obtained by integrating the bending energy up to the end of fusion-site (i.e. up to  $\rho = \rho_p - r_p$ ). As we can see, initially the total energy decreases quickly as the fusion-site radius increases. However, for larger values of ( $\rho_p - r_p$ ), the total energy remains almost independent of the size of fusion-site. The energy stored in the dimple-top reaches a maximum value at certain value of ( $\rho_p - r_p$ ). The maximum energy stored in the dimple-top, which facilitates the fusion process, occurs for the radius 2.75 nm of the fusion-site. We got, for the maximum energy stored in the dimple, the fusion-site radius is approximately equal to  $r_p$ . This result is consistent with the discussion in [15] that the inner-radius of the

cluster is comparable to the radius of HA-trimer forming the cluster.

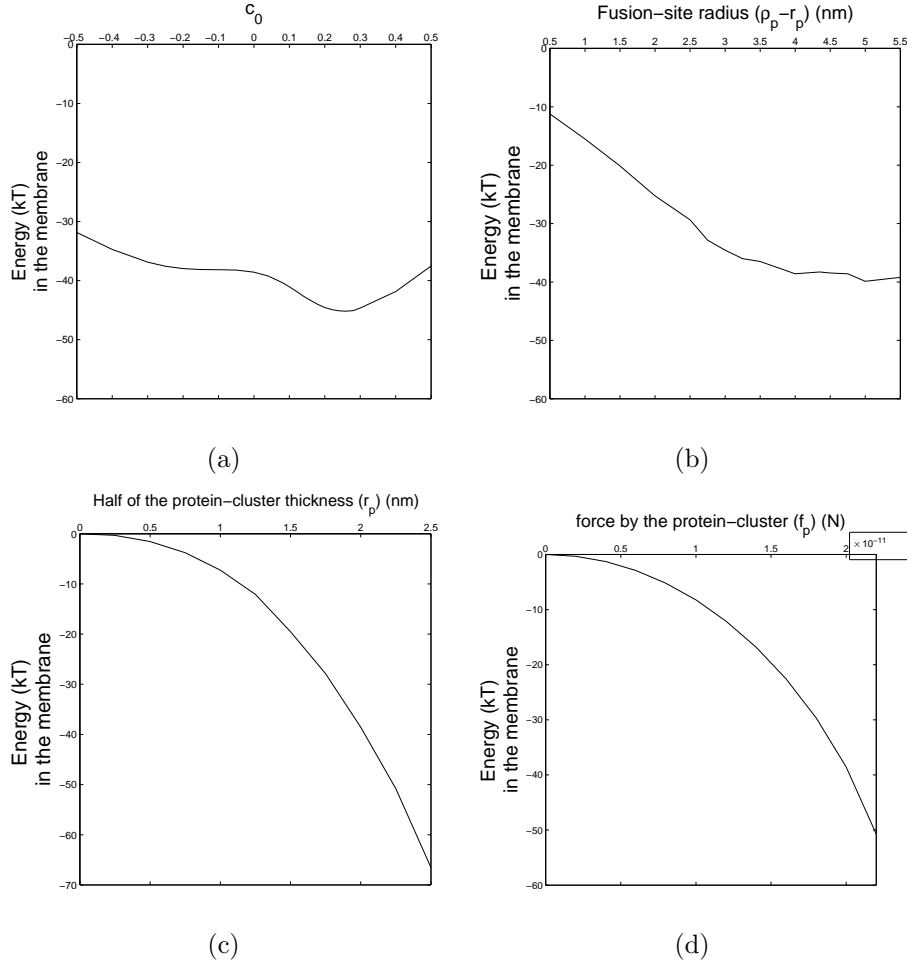


Figure 4: Energy in the entire membrane (i.e the membrane up to  $\rho = \rho_p + r_p$ ) depending on (a) the spontaneous curvature  $c_0$  (b) the fusion-site radius (c) the protein-cluster thickness (d) the force by the protein-cluster.

Now we examine the effect of the protein-cluster thickness ( $2r_p$ ) on the membrane deformation. We again set  $f_p = 2 \times 10^{-11}$  N,  $c_0 = 0$  and the fusion-site radius  $(\rho_p - r_p) = 4$  nm. As shown in Fig. 3(b), increasing the protein-cluster thickness increases the dimple height. While the total energy in the membrane (including bending as well as that due to the protein force) increases (in its absolute value) as the protein-cluster thickness increases, the bending energy in the dimple-top also increases with the protein-cluster thickness.

This is shown in Figs. 4(c) and 5(c). This result is also consistent with the conclusion made in [15].

In Fig. 3(c), we show that the height of the dimple grows when the force exerted by the protein-cluster increases. The total energy in the membrane and the bending energy in the dimple-top as functions of the protein force, while keeping  $c_0 = 0$ ,  $r_p = 2$  nm and  $(\rho_p - r_p) = 4$  nm, are plotted in Figs. 4(d) and 5(d), respectively. Again the magnitude of the total energy in the membrane is negative and the bending energy in the dimple-top is positive. Absolute value of the energy in the membrane and the energy in the dimple-top both increase with the force exerted by the protein-cluster.

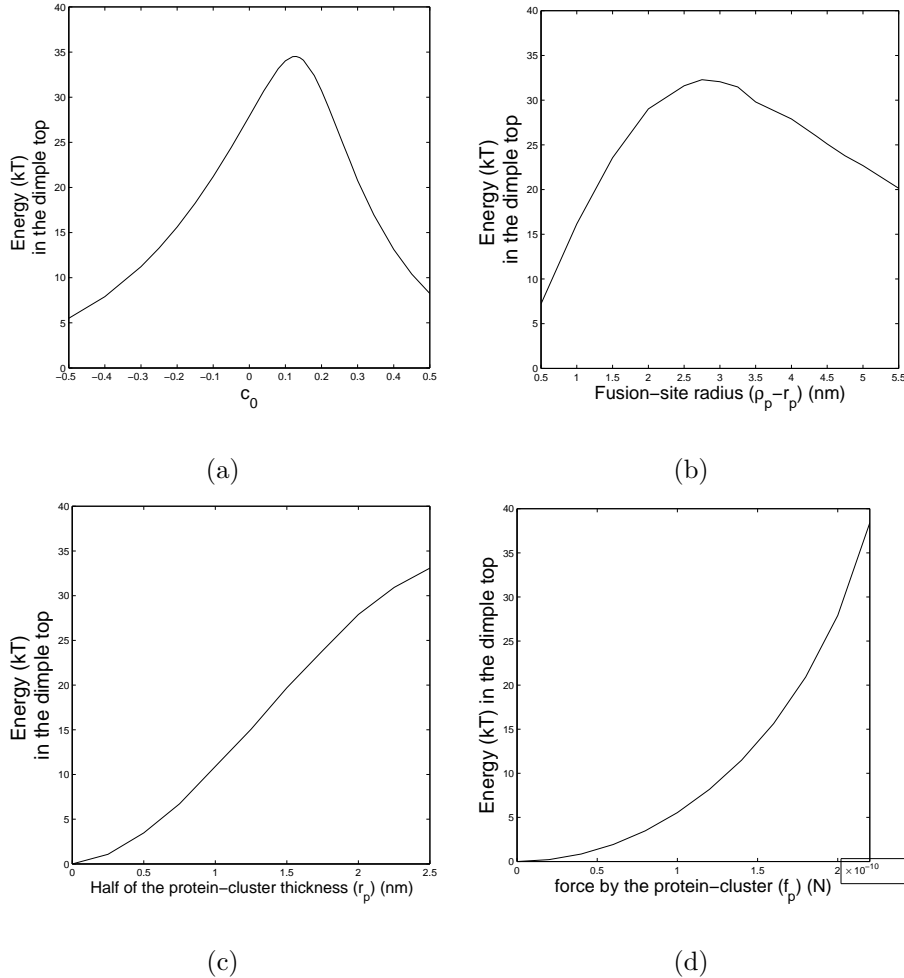


Figure 5: Energy in the dimple top (i.e the membrane up to  $\rho = \rho_p - r_p$ ) depending on (a) the spontaneous curvature  $c_0$  (b) the fusion-site radius (c) the protein-cluster thickness (d) the force by the protein-cluster.

The effect of spontaneous curvature  $c_0$  on the energy of the lipid bilayers is of very much interest for experimental works. In Figs 4(a) and 5(a), the total membrane energy and the bending energy in the dimple top are plotted for  $f_p = 2 \times 10^{-11}$  N,  $\rho_p = 6$  nm and  $r_p = 2$  nm. The total energy in the membrane decreases at first and then increases as  $c_0$  increases. Also, the bending energy stored in the dimple is not a monotonic function of  $c_0$ . The maximum value of the dimple bending energy occurs at a small positive value of  $c_0$ . Therefore, the small positive spontaneous curvature favors the fusion to occur. This result is in a very good agreement with the experiment [23]. In [23], it has been observed that the fusion does not occur in the presence of too much agents with positive spontaneous curvature, such as lysophosphatidylcholine (LPC), but the subsequent removal of LPC leads to fusion.

## 5.2 Incompressible membranes

To examine the effect of the incompressibility property of the biological membrane, we solve equations (3.10)-(3.11) and the result for  $f_p = 2.4 \times 10^{-11}$  N,  $\rho_p = 6$  nm and  $r_p = 2$  nm is presented in Fig. 6. Graphs are plotted for  $\gamma = 0, 3, 6, 10 \times 10^{-4}$  Nm<sup>-1</sup>. The plot for  $\gamma = 0$  Nm<sup>-1</sup> corresponds to the case without taking membrane compressibility into account. The graph clearly shows that there is an effect of the tension  $\gamma$  on the height of the dimple as well as on the energy stored in the dimple-top. Increase in the in-plane tension developed from 0 to  $10 \times 10^{-4}$  Nm<sup>-1</sup>, i.e., membrane becomes less compressible, reduces the height of the dimple as well as the energy stored in the dimple-top from 55.40 kT to 36.28 kT. Therefore, the incompressibility nature of the membrane causes the formation of dimple less favorable and so opposes the fusion to occur. This result strongly supports the experiment [23], which observed and concluded that the membrane tension prevents dimple formation and, therefore inhibits fusion.

## 5.3 Presence of the host cell

As discussed earlier, the presence of the host cell imposes a constraint on the maximum height of the viral membrane deformation. Fig. 7 (a) and (b), show the effect on the growing dimple when its height is constrained by the presence of the cell membrane. In Fig. 7 (a), the shape of the viral membrane is plotted

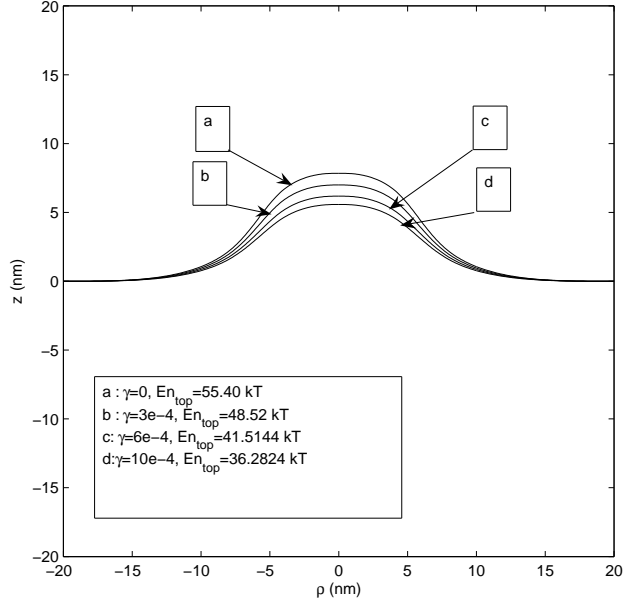


Figure 6: Contour graph of the viral membrane showing the effect of the membrane compressibility.

by setting the cell membrane constraints at the heights 4 nm, 3 nm, 2 nm and 1 nm from the  $\rho$ -axis. The graphs presented here are for the same protein force. Due to the presence of the cell membrane closer to the viral membrane, the dimple-top becomes flatter. In Fig. 7 (b), we vary the protein-force while fixing the maximum height. The viral membrane shape begins to become flatter when the protein-force is increased. With excessive force, the viral membrane leaves the cell membrane at the axis of symmetry forming a small reverse dimple. Therefore, the shape of the viral membrane in the presence of the cell membrane is determined by the height of the cell membrane location and the magnitude of the protein-force.

To understand the mixing of two membranes in detail two membranes in the bilayer have to be considered separately as monolayers with their coupling condition because during the fusion the outer and the inner monolayer of the bilayer behave in the different manner.

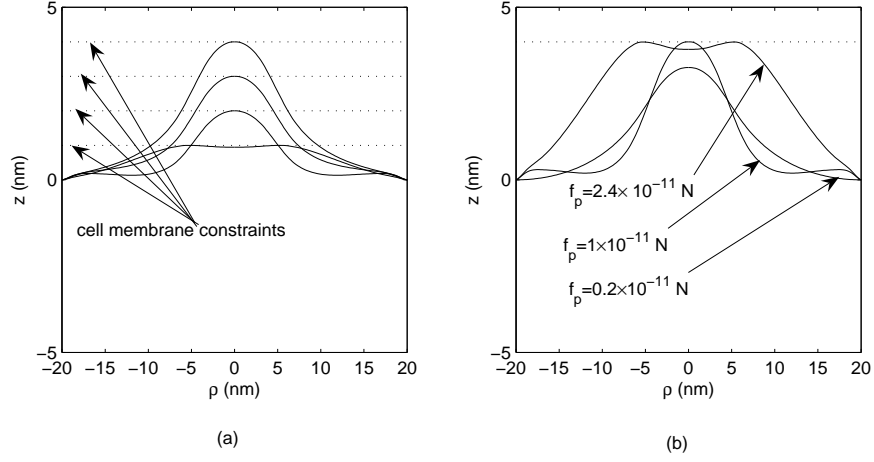


Figure 7: (a) Contour graph of the viral membrane with the cell membrane constraint at different heights. (b) Contour graph of the viral membrane for the different protein-forces under the fixed cell membrane constraint.

## 6 Conclusion

We present a mathematical model for the pre-fusion process in which HA-protein cluster brings the viral and cell membranes in close contact for fusion. A correct shape equation is derived using the method of Lagrangian multipliers.

Our results on dimple formation confirm the hypothesis in literature that the pre-fusion deformation can be mediated by the HA-protein clusters. Moreover, the energy stored in the dimple-top predicted by our model is at a physically reasonable level to facilitate the merging of the contacting monolayers. There exist values of the fusion-site radius and the spontaneous curvature corresponding to optimal dimple height and optimal energy stored in the dimple-top. The dimple height and the energy stored in the dimple-top have positive correlation with the protein-cluster thickness and the protein-force. The incompressibility property of the membrane also plays a role in determining the shape of the membrane as well as the energy stored in the dimple-top. Less compressible membranes resist more strongly towards bending thereby reduce the chance for the membranes to come closer and to fuse with each other. Effect of incompressibility property

and spontaneous curvature produced by our model is in a good agreement with the experimental observations. The shape of the viral membrane constrained by the presence of the cell membrane depends upon the location of the cell membrane as well as the magnitude of the protein force. For a more detailed understanding of the merging phenomena of two approaching membranes, our model needs to be generalized by considering individual monolayers.

**Acknowledgement.** Part of the research is supported by the Natural Science and Engineering Research Council (NSERC) of Canada. One of the authors (HH) also wish to thank Japan Society for the Promotion of Sciences (JSPS) for providing a visiting fellowship while part of this research was carried out.

## References

- [1] BENTZ, J., ELLENS, H. AND ALFORD, D. (1990) An architecture for the fusion site of influenza hemagglutinin. *FEBS Lett.*, **276**, 1-5.
- [2] BLUMENTHAL, R., CLAGUE, M. J., DURELL, S. R. AND EPAND, R. M. (2003) Membrane fusion. *Chemical Review*, **103**, 53-69.
- [3] Blumenthal, R., Pak, C. C., Raviv, Y., Krumbiegel, M., Bergelson, L. D., Morris, S. J. and Lowy, R. J. (1995) Transient domains induced by influenza hemagglutinin during membrane fusion. *Mol. Membr. Biol.*, **12**, 135-142.
- [4] Blyth, M. G. and Pozrikidis, C. (2004) Solution space of axisymmetric capsules enclosed by elastic membranes. *European Journal of Mechanics A/Solids*, **23**, 877-892.
- [5] Boal, D. (2002) *Mechanics of the cell*. Cambridge University Press, Cambridge, UK.
- [6] Danieli, T., Pelletier, S. L., Henis, Y. I. and White, J. M. (1996) Membrane fusion mediated by the influenza virus hemagglutinin requires the concerted action of atleast three hemagglutinin trimers. *J. Cell Biol.*, **133**, 559-569.

- [7] Eckert, D. M. and Kim, P. S. (2001) Mechanisms of viral membrane fusion and its inhibition. *Annu. Rev. Biochem.*, **70**, 777-810.
- [8] Gaudin, Y., Ruigrok, R. W. H. and Brunner, J. (1995) Low-pH induced conformational changes in viral fusion proteins: implications for the fusion mechanism. *Journal of Gen. Virol.*, **76**, 1541-1556.
- [9] Gruenke, J. A., Armstrong, R. T., Newcomb, W. W., Brown, J. C. and White, J. M. (2002) New insights into the spring-loaded conformational change of influenza virus hemagglutinin. *Journal of Virology*, **76** (9), 4456-4466.
- [10] Gutman, O., Danieli, T., White, J. M. and Henis, Y. I. (1993) Effects of exposure to low pH on the lateral mobility of influenza hemagglutinin expressed at the cell surface: correlation between mobility inhibition and inactivation. *Biochemistry*, **32**, 101-106.
- [11] Helfrich, W. (1973) *Z. Naturforsch.*, **28c**, 693.
- [12] Hu, J.-G. and Ou-Yang, Z.-C. (1993) Shape equations of the axisymmetric vesicles. *Physical Review E*, **47**(1), 461-467.
- [13] Julicher, F. and Seifert, U. (1994) Shape equations for axisymmetric vesicles: a clarification. *Physical Review E*, **49**(5), 4728-4731.
- [14] Komura, S. (1996) Shape fluctuations of Vesicles. *Vesicles*. Marcel Dekker, New York, 198-236.
- [15] Kozlov, M. M. and Chernomordik, L. V. (1998) A mechanism of protein-mediated fusion: coupling between refolding of the influenza hemagglutinin and lipid rearrangements. *Biophysical Journal*, **75**, 1384-1396.
- [16] Kozlov, M. M. and Chernomordik, L. V. (2002) The protein coat in membrane fusion: Lessons from fission. *Traffic Interchange*, **3**, 256-267.
- [17] Kozlovsky, Y., Chernomordik, L. V. and Kozlov, M. M. (2002) Lipid intermediates in membrane fusion: formation, structure and decay of hemifusion diaphragm. *Biophysical Journal*, **83**, 2634-2651.

- [18] Kozlovsky, Y. and Kozlov, M. M. (2002) Stalk model of membrane fusion: solution of energy crisis. *Biophysical Journal*, **82**, 882-895.
- [19] Kuzmin, P. I., Zimmerberg, J., Chizmadzhev, Y. A. and Cohen, F. S. (2001) A quantitative model for membrane fusion based on low-energy intermediates. *PNAS*, **98** (13), 7235-7240.
- [20] Li, Y., Han, X., Lai, A. L., Bushweller, J. H., Cafiso, D. S. and Tamm, L. K. (2005) Membrane structures of the hemifusion-inducing fusion peptide mutant G1S and the fusion-blocking mutant G1V of influenza virus hemagglutinin suggest a mechanism for pore opening in membrane fusion. *Journal of Virology*, **79** (18), 12065-12076.
- [21] Markin, V. S and Albanesi, J. P. (2002) Membrane fusion: Stalk model revisited. *Biophysical Journal*, **82**, 693-712.
- [22] Markovic, I., Leikina, E., Zhukovsky, M., Zimmerberg, J. and Chernomordik, L. V. (2001) Synchronized activation and refolding of influenza hemagglutinin in multimeric fusion machines. *The Journal of Cell Biology*, **155** (5), 833-843.
- [23] Markosyan, R. M., Melikyan, G. B. and Cohen, F. S. (1999) Tension of membranes expressing the Hemagglutinin of influenza virus inhibits fusion. *Biophysical Journal*, **77**, 943-952.
- [24] May, S. (2002) Structure and energy of fusion stalks: the role of membrane edges. *Biophysical Journal*, **83**, 2969-2980.
- [25] Naito, H., Okuda, M. and Ou-Yang, Z.-C. (1993) Counterexample to some shape equations for axisymmetric vesicles. *Physical Review E*, **48** (3), 2304-2307.
- [26] Pozrikidis, C. (2005) Resting shape and spontaneous membrane curvature of red blood cells. *Mathematical Medicine and Biology*, **22**, 34-52.
- [27] Pozrikidis, C. (2003) Shell theory for capsules and cells. *Modeling and Simulation of Capsules and Biological Cells*. Chapman & Hall/CRC, 35-101.

- [28] Sage, A. P. (1968) *Optimal Systems Control*. Prentice-Hall, Inc., N.J.
- [29] Skehel, J. J. and Wiley, D. C. (2000) Receptor binding and membrane fusion in virus entry: the influenza haemagglutinin. *Annu. Rev. Biochem.*, **69**, 531-569.
- [30] Stegmann, T. (1993) Influenza hemagglutinin-mediated membrane fusion does not involve inverted phase lipid intermediates. *Journal of Biol. Chem.*, **268**, 1716-1722.
- [31] Spivak, M. (1997) *A Comprehensive Introduction to Differential Geometry*. Publish or Perish, Berkeley.
- [32] Tamm, L. K., Abildgaard, F., Arora, A., Blad, H., Bushweller, J. H. (2003) Structure, dynamics and function of the outer membrane protein A (OmpA) and influenza hemagglutinin fusion domain in detergent micelles by solution NMR. *FEBS Letters*, **555**, 139-143.
- [33] Tamm, L. K. (2003) Hypothesis: spring-loaded boomerang mechanism of influenza hemagglutinin-mediated membrane fusion. *Biochimica et Biophysica Acta*, **1614**, 14-23.
- [34] Tamm, L. K., Crane, J. and Kiessling, V. (2003) Membrane fusion: a structural perspective on the interplay of lipids and proteins. *Current Opinion in Structural Biology (Elsevier)*, **13**, 453-466.
- [35] Willmore, T. J. (1982) *Total Curvature in Riemannian Geometry*. Horwood Ltd., Chichester.
- [36] Wiley, D. C. and Skehel, J. J. (1987) The structure and function of the hemagglutinin membrane glycoprotein of influenza virus. *Ann. Rev. Biochem.*, **56**, 365-394.
- [37] Zheng, W. and Liu, J. (1993) Helfrich shape equation for axisymmetric vesicles as a first integral. *Physical Review E*, **48** (4), 2856-2860.
- [38] Ou-Yang, Z.-C. and Helfrich, W. (1989) Bending energy of vesicle membranes: general expressions for the first, second and third variation of the shape energy and applications to spheres and cylinders. *Physical Review A*, **39** (10), 5280-5288.
- [39] Zimmerberg, J., Vogel, S. S. and Chernomordik, L. V. (1993) Mechanism of membrane fusion. *Annu. Rev. Biophys. Biomol. Struct.*, **22**, 433-466.

## Appendix. Derivation of the correct axisymmetric shape equations

For incompressible vesicles (closed lipid bilayer membranes) with a fixed area to volume ratio, the equilibrium shape can be determined by minimizing the bending energy given by the spontaneous-curvature model of Helfrich [11, 38]:

$$F = \frac{1}{2}k_b \oint (c_1 + c_2 - c_0)^2 dA + k_G \oint c_1 c_2 dA + \lambda \oint dA + \Delta P \int dV \quad (\text{A.1})$$

where  $dA$ ,  $k_b$ ,  $k_G$ ,  $c_1$ ,  $c_2$  and  $c_0$  are the same as in the viral membrane model and  $dV$  is the volume element;  $\lambda$  and  $\Delta P$  are Lagrangian multipliers used to incorporate the constraints of constant area and constant volume respectively. Physically  $\lambda$  and  $\Delta P$  can be interpreted as the tensile stress and the pressure difference respectively. For vesicles with the same topological forms, the Gaussian curvature term  $k_G \oint c_1 c_2 dA$  can be dropped from (A.1).

The general shape equation derived by Ou-Yang and Helfrich [38], which is widely accepted as the correct shape equation, is

$$\Delta P - 2\lambda H + k_b(2H + c_0)(2H^2 - 2K - c_0 H) + 2k_b \nabla^2 H = 0$$

where  $\nabla^2$  is the Laplace-Beltrami operator on the surface. Substituting the axisymmetric curvature expressions into the general equation, the shape equation can be obtained as [4, 12, 25, 27, 37]:

$$\begin{aligned} \cos^3 \psi \frac{d^3 \psi}{d\rho^3} &= 4 \sin \psi \cos^2 \psi \frac{d^2 \psi}{d\rho^2} \frac{d\psi}{d\rho} - \cos \psi (\sin^2 \psi - \frac{1}{2} \cos^2 \psi) \left( \frac{d\psi}{d\rho} \right)^3 + \frac{7 \sin \psi \cos^2 \psi}{2\rho} \left( \frac{d\psi}{d\rho} \right)^2 \\ &\quad - \frac{2 \cos^3 \psi}{\rho} \frac{d^2 \psi}{d\rho^2} + \left( \frac{c_0^2}{2} - \frac{2c_0 \sin \psi}{\rho} + \frac{\sin^2 \psi}{2\rho^2} + \frac{\lambda}{k_b} - \frac{\sin^2 \psi - \cos^2 \psi}{\rho^2} \right) \cos \psi \frac{d\psi}{d\rho} \\ &\quad + \frac{\Delta P}{k_b} + \frac{\lambda \sin \psi}{k_b \rho} - \frac{\sin^3 \psi}{2\rho^3} + \frac{c_0^2 \sin \psi}{2\rho} - \frac{\sin \psi \cos^2 \psi}{\rho^3}. \end{aligned} \quad (\text{A.2})$$

### A.1 Variation in $\rho$ -direction

We derive the shape equation for axisymmetric vesicles by taking the variation of the axisymmetric energy functional. The method used here is similar to [12] but the variation is performed along the direction

perpendicular to the axis of symmetry (i.e.  $\rho$  direction) and the corresponding induced variations in  $\psi$  and  $s$  are obtained by using the geometric relations (3.1) and (3.2). The method used here is similar to the method used to find the equation of geodesics in Riemannian geometry by means of the variational method [12, 31].

We start with the following axisymmetric shape energy functional with parameter  $s$

$$F_s = \pi \int \left[ k_b \rho \left( \frac{d\psi}{ds} + \frac{\sin \psi}{\rho} - c_0 \right)^2 + \Delta P \rho^2 \sin \psi + 2\lambda \rho \right] ds \quad (\text{A.3})$$

and introduce an arbitrary parameter  $t$  to get

$$F_s = \pi \int \bar{L}(\rho(t), \psi(t), \dot{\psi}(t), \dot{s}(t)) dt, \quad (\text{A.4})$$

where

$$\begin{aligned} \bar{L}(\rho(t), \psi(t), \dot{\psi}(t), \dot{s}(t)) &= k_b \rho \left( \frac{\dot{\psi}}{\dot{s}} + \frac{\sin \psi}{\rho} - c_0 \right)^2 \dot{s} + \Delta P \rho^2 \sin \psi \dot{s} + 2\lambda \rho \dot{s}, \\ \dot{\psi}(t) &= \frac{d\psi}{dt} \\ \dot{s}(t) &= \frac{ds}{dt}. \end{aligned} \quad (\text{A.5})$$

Terms  $2k_b \dot{\psi} \sin \psi$  and  $-2k_b c_0 \dot{s} \sin \psi$  in (A.5) do not contribute to the shape equation [12], so we neglect them and work with the following Lagrangian

$$\begin{aligned} \bar{L}(\rho(t), \psi(t), \dot{\psi}(t), \dot{s}(t)) &= \frac{k_b \rho (\dot{\psi})^2}{\dot{s}} + \frac{k_b \dot{s} \sin^2 \psi}{\rho} + k_b \rho c_0^2 \dot{s} - 2k_b c_0 \rho \dot{\psi} + 2\lambda \rho \dot{s} \\ &+ \Delta P \rho^2 \sin \psi \dot{s}. \end{aligned} \quad (\text{A.6})$$

Let  $\delta\rho$  be the infinitesimal variation along the  $\rho$ -direction so that the variation along the  $z$ -direction is  $\delta z = 0$  (See Fig. 8). From the geometric relation (3.1), we have  $d\rho = \cos \psi ds$  which gives

$$-\sin \psi ds(\delta\psi) + \cos \psi \delta ds = \delta d\rho. \quad (\text{A.7})$$

Similarly, from the geometric relation (3.2), we have  $dz = -\sin \psi ds$  which, using  $d\delta z = \delta dz$  due to independence between operators  $d$  and  $\delta$ , gives

$$\cos \psi ds(\delta\psi) + \sin \psi \delta(ds) = 0. \quad (\text{A.8})$$

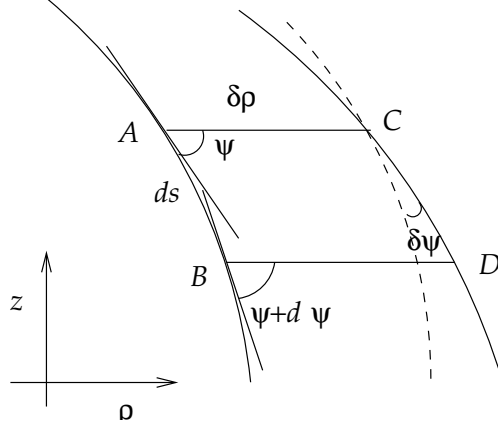


Figure 8: The variation in the direction perpendicular to the axis of symmetry (i.e in  $\rho$ -direction).  $AB = ds$  is the segment in the original generating curve,  $CD$  is the corresponding segment in the curve deduced by the variation  $\delta\rho$  in  $\rho$ -direction and dashed curve is the curve deduced by moving the original curve from  $A$  to  $C$ .

Solving Equations (A.7) and (A.8) for  $\delta\psi$  and  $\delta(ds)$ , we get

$$\delta\psi = -\frac{\sin\psi\delta d\rho}{ds}, \quad (\text{A.9})$$

$$\delta(ds) = \cos\psi\delta d\rho, \quad (\text{A.10})$$

and also

$$\delta\dot{\psi} = -\frac{d}{dt}\left(\frac{\sin\psi\delta d\rho}{ds}\right), \quad (\text{A.11})$$

$$\delta\dot{s} = \frac{\cos\psi\delta d\rho}{dt}. \quad (\text{A.12})$$

The shape equation is determined by the variational equation  $\delta F_s = 0$ , which gives

$$\int \left[ \frac{\partial \bar{L}}{\partial \rho} \delta\rho + \frac{\partial \bar{L}}{\partial \psi} \delta\psi + \frac{\partial \bar{L}}{\partial \dot{\psi}} \delta\dot{\psi} + \frac{\partial \bar{L}}{\partial \dot{s}} \delta\dot{s} \right] dt = 0. \quad (\text{A.13})$$

Using Equations (A.9), (A.11) and (A.12) in (A.13) and performing integration by parts and simplification, we obtain the following shape equation

$$\frac{\partial \bar{L}}{\partial \rho} + \frac{d}{dt} \left( \frac{\sin\psi}{\dot{s}} \frac{\partial \bar{L}}{\partial \psi} \right) - \frac{d}{dt} \left( \frac{\sin\psi}{\dot{s}} \frac{d}{dt} \frac{\partial \bar{L}}{\partial \dot{\psi}} \right) - \frac{d}{dt} \left( \cos\psi \frac{\partial \bar{L}}{\partial \dot{s}} \right) = 0. \quad (\text{A.14})$$

After using Equation (A.6) in (A.14) and simplifying, we end up with the following shape equation

$$\begin{aligned}
\frac{k_b \rho}{(\dot{s})^2} \frac{d^3 \psi}{dt^3} &= \frac{3k_b \rho \ddot{s}}{(\dot{s})^3} \ddot{\psi} - \frac{2k_b \dot{\rho}}{(\dot{s})^2} \ddot{\psi} + \frac{k_b (\dot{s} - \dot{\rho} \cos \psi)}{2\dot{s}^2 \sin \psi} (\dot{\psi})^2 - \frac{k_b \rho}{2(\dot{s})^2} (\dot{\psi})^3 \\
&+ \left[ \frac{k_b (2 - 3 \sin^2 \psi)}{2\rho} - \frac{k_b \ddot{\rho}}{(\dot{s})^2} + \frac{k_b \rho (d^3 s / dt^3)}{(\dot{s})^3} - \frac{3k_b \rho (\dot{s})^2}{(\dot{s})^4} + \frac{3k_b \dot{\rho} \ddot{s}}{(\dot{s})^3} + \lambda \rho \right. \\
&- \left. \frac{k_b c_0}{\sin \psi} + \frac{k_b c_0 \cos \psi \dot{\rho}}{\dot{s} \sin \psi} + \frac{k_b c_0^2 \rho}{2} \right] \dot{\psi} \\
&+ \Delta P \rho \dot{s} + \left( \frac{\dot{s}}{\sin \psi} - \frac{\dot{\rho} \cos \psi}{\sin \psi} \right) \lambda - \frac{k_b \dot{s} \sin \psi}{2\rho^2} - \frac{k_b \sin \psi \cos \psi \dot{\rho}}{2\rho^2} \\
&+ \frac{k_b c_0^2 (\dot{s} - \dot{\rho} \cos \psi)}{2 \sin \psi} + \frac{k_b c_0 \ddot{\rho}}{\dot{s}} - \frac{k_b c_0 \dot{\rho} \ddot{s}}{(\dot{s})^2}
\end{aligned} \tag{A.15}$$

We now consider  $\rho$  as a parameter by taking  $t = \rho$ . Then using  $\dot{\psi} = d\psi/d\rho$ ,  $\dot{s} = ds/d\rho = 1/\cos \psi$ ,  $\dot{\rho} = 1$  along with their higher derivatives in (A.15), we obtain (A.2). Therefore, we have shown that the variation does not have to be in the normal direction, the variation in the other direction than the normal direction can also produce the same shape equation if the induced variations in other variables are obtained by using the geometric relations (3.1) and (3.2). We note that the approach outlined here breaks down when the surface is perpendicular to the axis of symmetry. More general approach is provided below.

## A.2 The method of Lagrangian Multiplier

We include the geometric condition  $\cos \psi (dz/d\rho) = \sin \psi$  in the action form of shape energy functional via an additional Lagrange multiplier  $\eta$  as follows:

$$F = \pi \int \tilde{L} \left( \rho, \psi(\rho), z(\rho), \eta(\rho), \frac{d\psi}{d\rho}, \frac{dz}{d\rho} \right) d\rho, \tag{A.16}$$

where the Lagrangian  $\tilde{L}(\rho, \psi(\rho), z(\rho), \eta(\rho), d\psi/d\rho, dz/d\rho)$  is

$$\begin{aligned}
\tilde{L} \left( \rho, \psi(\rho), z(\rho), \eta(\rho), \frac{d\psi}{d\rho}, \frac{dz}{d\rho} \right) &= \frac{k_b \rho}{\cos \psi} \left( \frac{d\psi}{d\rho} \cos \psi + \frac{\sin \psi}{\rho} - c_0 \right)^2 + \frac{\Delta P \rho^2 \sin \psi}{\cos \psi} + \frac{2\lambda \rho}{\cos \psi} \\
&+ \eta \left( \frac{dz}{d\rho} \cos \psi + \sin \psi \right).
\end{aligned} \tag{A.17}$$

From the Euler-Lagrange equation

$$\frac{\partial \tilde{L}}{\partial \Phi} - \frac{d}{d\rho} \frac{\partial \tilde{L}}{\partial (d\Phi/d\rho)} = 0$$

for  $\Phi = \psi, \eta$  and  $z$ , we obtain the following system of equations

$$\begin{aligned} \cos^2 \psi \frac{d^2 \psi}{d\rho^2} &= \frac{\sin \psi \cos \psi}{2} \left( \frac{d\psi}{d\rho} \right)^2 + \frac{\sin \psi}{2\rho^2 \cos \psi} + \frac{\sin \psi \cos \psi}{2\rho^2} + \frac{c_0^2 \sin \psi}{2 \cos \psi} - \frac{\cos^2 \psi}{\rho} \frac{d\psi}{d\rho} - \frac{c_0}{\rho \cos \psi} \\ &+ \frac{\Delta P \rho}{2k_b \cos \psi} + \frac{\lambda \sin \psi}{k_b \cos \psi} + \frac{c_0 \cos \psi}{\rho} + \frac{\eta}{2k_b \rho}, \end{aligned} \quad (\text{A.18})$$

$$\frac{dz}{d\rho} = -\frac{\sin \psi}{\cos \psi}, \quad (\text{A.19})$$

$$\cos \psi \frac{d\eta}{d\rho} = \eta \sin \psi \frac{d\psi}{d\rho}. \quad (\text{A.20})$$

We rewrite (A.18) as  $\eta = \eta(\rho, \psi, d\psi/d\rho, d^2\psi/d\rho^2)$  and find the expression for  $d\eta/d\rho$ . Then we substitute the expressions for  $\eta$  and  $d\eta/d\rho$  in (A.20). After lengthy mathematical manipulations, we obtain (A.2), which is the correct shape equation.